

## Making Use of Labyrinth Interaction Flow

Pfau A., Kalfas A.I., Abhari R.S.  
Turbomachinery Laboratory  
Swiss Federal Institute of Technology  
8092 Zurich, Switzerland  
pfau@lsm.iet.mavt.ethz.ch

### ABSTRACT

It is the aim of this publication to attract the designers attention to the end wall flow interactions of shrouded high pressure turbines. One of the key issue for designing better turbines is the understanding of the flow interactions set up by the presence of labyrinth seals. Those interaction flows are carefully examined in this publication using the control volume analysis and the radial equilibrium of forces acting on streamlines. The consequences on secondary flow development and mixing losses are discussed and quantified. Out of this insight, design recommendations are derived, which attempt to make use of the nature of the labyrinth interaction flow.

The open labyrinth cavities are classified in a systematic way. The aim of this approach is to work out the characteristic differences between hub and tip cavities and those having a leakage jet or sucking main flow fluid into the labyrinth. The influence on the main flow is discussed in terms of the incidence flow angle of downstream blade rows and the associated loss production mechanisms.

The design strategies presented in this paper follow two paths: (a) Optimization of the mixing losses of the leakage jets at hub and tip is estimated to result in an efficiency increase of up to 0.2%. (b) The non-axisymmetric shaping of the labyrinth interaction flow path aims at the secondary flow control in downstream blade rows. This approach might contribute in the same magnitude of order as the reduction in the mixing losses.

### NOMENCLATURE

|                |   |
|----------------|---|
| $r, \theta, z$ | cylindrical coordinate system   |
| $g$            | radial gap width in % of blade height                                 |
| $h$            | blade height, 90mm  |
| $z_{cav}$      | axial cavity width, 15mm  |
| $n$            | numbers of blades, 42   |
| $f_{blade}$    | blade passing frequency   |
| $M$            | Mach-number   |
| $p$            | local blade pitch, $2\pi r/42$  |
| $R$            | non-dimensional radial height $\frac{r - r_{Hub}}{r_{Tip} - r_{Hub}}$ |

|          |   |
|----------|---|
| $Re$     | Reynolds-number   |
| $s$      | specific entropy  |
| $T$      | blade passing period $1/f_{blade}$ , temperature  |
| $U$      | local blade speed   |
| $Z$      | non-dimensional axial distance $z/z_{cav}$  |
| $v$      | non-dimensional velocity $u_{loc}/U$  |
| $C_p$    | non-dimensional pressure $C_p = \frac{P_{local} - P_{stat,out}}{P_{total,in} - P_{stat,out}}$ |
| $\alpha$ | absolute yaw angle  |
| $\beta$  | relative flow angle   |
| $\Omega$ | non-dimensional vorticity $\omega/(4\pi f_{blade})$   |
| $\Theta$ | non-dimensional circumferential position $\theta/p$   |

### Indices

|     |                      |
|-----|----------------------|
| G   | maximum gap position |
| H   | hub                  |
| i   | inner                |
| L   | leakage jet          |
| o   | outer                |
| rel | relative system      |
| T   | tip                  |

### Abbreviations

|      |                                  |
|------|----------------------------------|
| TC03 | 0.3% seal gap case ( $g=0.3\%$ ) |
| TC1  | 1% gap case ( $g=1\%$ )          |
| FRAP | fast response aerodynamic probe  |

### INTRODUCTION

Labyrinth leakage flow in shrouded turbines is looked upon as an inherently detrimental effect and something which the designer cannot avoid. One design recommendation is to minimize the leakage flow through designing better labyrinth seals and to reduce the gap widths as much as possible. If heat transfer is an issue as in a gas turbine the gap must allow enough leakage mass flow in order to cool the turbine shrouds. The inlet to a labyrinth and the exit including the leakage jet alter the flow field in turbine end wall regions. This is of special significance in low aspect ratio turbine stages where secondary flows

are strong. The labyrinth seal can be optimized for itself including mechanical limits and through flow coefficients.

The subject of cavity interactions in turbines was initially addressed the first time by Denton and Johnson [1]. However, it is only in recent years that this subject attracted the attention of the turbomachinery research community. Peters et al. [2] examined the effect of gap size on the steady interaction between the leakage flow and the secondary flow field of a subsequent stator in a 1.5 stage, shrouded axial turbine. Hunter and Manwaring [3] reported about two extra vortices generated in a downstream stator blade row. Wallis et al. [4] observed that strong interactions are present in open cavities of shrouded turbine blades. The following blade rows were found to receive the tip flow at a negative incidence. Anker and Mayer [5] numerically investigated the leakage interaction with the main flow and found, that the tip leakage flow is not uniform in the pitch wise direction. Schlienger et al. [6] changed the geometry of the labyrinth exit cavities by introducing inserts and compared the effects on the main flow as well as on the efficiency. These studies have focussed mainly on the interaction occurring in the main flow and following blade passages.

However, as the origins of these interactions are open cavities, an increased emphasis should be placed on the associated steady and unsteady flow interactions within these cavities. From these considerations the question arises: Is there any potential in improving the overall performance of low aspect ratio, shrouded turbines by looking at the combined system of main flow duct and labyrinth seal? In that respect, the present publication attempts to conclusively summarize and complete the work which already has been published in [7] and [8]. It is the aim of this publication to give an overview of labyrinth interaction effects occurring in shrouded turbines with large inlet and exit cavities. Additionally, all open cavities are treated in a systematic way and effects on the main flow are discussed and quantified. Based on the detailed flow understanding, which was experimentally gained in a two stage, shrouded, low speed turbine, new design features are derived for a range of open cavities. With this step, design modifications are proposed, which actually make use of the labyrinth interaction flows.

## TEST RIG, MEASUREMENT TECHNOLOGY AND DATA SET

The cavity interaction flow was investigated in the 2-stage low speed axial turbine 'LISA'. The test rig is described in detail in Sell et al. [9]. The main characteristics of the turbine are summarized in table 1.

The constant annulus of the turbine and the four blade rows are depicted in figure 1. The stepped shrouds on the blades together with three sealing fins form the labyrinth seal. The geometry under investigation is similar to steam turbine applications, where large inlet and exit cavities allow for axial displacement of the rotor shaft due to thermal expansion of the rotor. Consequently, the blade profiles are of a medium loaded type with 50% reaction and leaned stator blades. The cylindrical coordinate system used in this publication is indicated in figure 1. The results are presented looking upstream as the observer indicates. The cavities are numbered for an easier identification in later discussions.

The measurement technology applied where a miniature five hole probe of 0.9mm head diameter and a virtual four sensor probe of 0.84mm head diameter. The accuracy of the five hole probe readings is discussed in detail in [10]. The corresponding error bars are given in

the diagrams. In [11] the virtual four sensor probe is described in detail. The advantages of this measurement technology are:

- 1) Very small head, minimizing blockage.
- 2) Three-dimensional flow vector.
- 3) Unsteady total and static pressure field.
- 4) Temporal resolution of the flow field up to 25kHz.

The results gained with the five-hole probe are considered to be the time averaged picture. A comparison to the virtual four sensor probe showed that this is a justifiable assumption ([11]).

A seal gap variation was performed covering two aspects:

a) The first gap variation of 1% blade height is close to the range found in real applications and a realistic flow field in terms of leakage jet strength and mixing can be expected.

b) As second case, a smaller gap width of 0.3% blade height was chosen to investigate the pure main flow to cavity interaction in a more controlled approach.

|                          |            |                           |                 |
|--------------------------|------------|---------------------------|-----------------|
| <b>Pressure ratio</b>    | 1.32       | <b>Mass flow</b>          | 9.86kg/s        |
| <b>Max. power</b>        | 400kW      | <b>Turbine speed</b>      | 2700rpm         |
| <b>T<sub>inlet</sub></b> | 40°C       | <b>P<sub>exit</sub></b>   | ambient         |
| <b>Mach</b>              | 0.1... 0.4 | <b>Re<sub>Cax</sub></b>   | 10 <sup>5</sup> |
| <b>n (rotor/stator)</b>  | 42         | <b>Tip diameter</b>       | 800mm           |
| <b>blade passing</b>     | 1890Hz     | <b>Blade aspect ratio</b> | 1.8             |

Table 1 Main characteristics of the test turbine

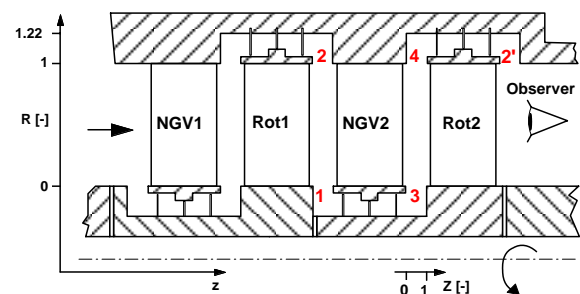


Figure 1 Meridional cut of the test section

The experiments were performed at a rotational speed of 2700rpm and a mass flow of 9.86kg/s. In real steam turbines the fluid dynamic conditions are  $Re=3 \cdot 10^6$  and  $M=0.3$  with a suction peak velocity of around  $M=0.8$ . Therefore, compressibility as well as viscous effects are not fully modelled in this turbine. However, as the velocity triangles and reduced frequencies match to an actual stage, unsteady effects like vortex or potential field interactions are comparable.

In table 2 the numbers of axial measurement planes in each cavity measured with the five-hole probe (time averaged) and measured with the virtual four sensor probe (time resolved) are listed. Most cavities are resolved with one measurement plane containing roughly of 350 measurement points. The single plane was positioned in mid axial gap position ( $Z=0.5$ ). Cavity 4 was resolved with 6 time averaged and 5 time resolved measurement planes in the 0.3% gap case having an average spacing of  $\Delta Z=0.15$ .

| Cavity   | 1 | 2   | 3   | 4   | 2'  |
|----------|---|-----|-----|-----|-----|
| 1% gap   | - | 1+1 | 1+0 | 1+1 | 1+1 |
| 0.3% gap | - | 1+1 | 1+1 | 6+5 | 1+1 |

Table 2 Numbers of axial measurement planes: 1+1, 1 plane time averaged, 1 plane time resolved

## EXPERIMENTAL RESULTS AND DISCUSSION

### Cavity 2 (outlet, tip)

#### Pitch-wise mass averaged results

First, a short comparison between the velocity fields of the 0.3% and 1% gap case of the seal gap variation is given in figure 2. The diagram shows the pitch-wise mass averaged tangential and axial velocity components. The black bars indicate the errors of the five hole probe measurement chain. The error bars vary with radial height, since the error depends on the flow angle and the Mach-number. For the 0.3% gap case the influence of the leakage jet onto the flow field at this location is negligible. The weak jet mixes out quickly downstream of the last seal and is not detected in the velocity profiles. In contrast, the leakage jet in the 1% gap case alters considerably the flow field due to its stronger mass and momentum flux. The leakage fluid can be localized in a radial band from  $R=1.03$  to  $R=1.07$ . For further investigations in this section the authors concentrate on the 1% gap case, where mixing and interaction flows are more realistic, than in the 0.3% gap case.

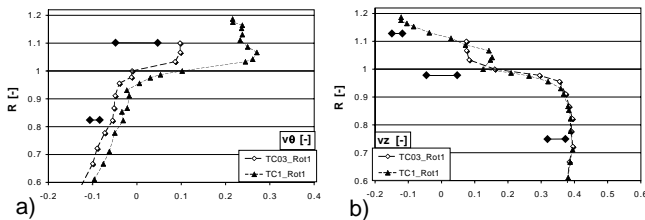


Figure 2 Pitch-wise mass averaged velocity profiles, cavity 2,  $Z=0.5$ : a) tangential, b) axial

#### Rotor relative, time averaged results

The unsteady data sets taken in cavity 2 are post-processed to the time-averaged picture in the relative frame of reference. The static pressure (figure 3), the relative Mach-number (figure 4), and the radial velocity component (figure 5) were chosen for display and discussion. The arrows indicate the sense of rotation of the relative coordinate system. The curved dashed line indicates the tip radius of the turbine blades. The shroud trailing edge reaches from  $R=1$  to  $R=1.06$ . The discussions of the results within this section happen in the relative frame, if not stated otherwise.

The static pressure distribution (figure 3) reveals the trailing edge position of the rotor blade at  $\Theta_{rel}=-0.3$  (dashed line), where a high static pressure is induced. The circumferential pressure variation from high to low pressure at  $\Theta_{rel}=0.3$  in the main flow region is also seen in the cavity. A stripe of higher static pressure at the radial position of the leakage jet ( $R=1.06$ ) is found. The circumferential variation at  $R=1.06$

is such that a low pressure region occurs at  $\Theta_{rel}=0.38$ . In addition, the level of static pressure within the cavity is on average  $\Delta C_{ps}=0.01$  higher than in the main flow. The circumferential static pressure distribution is imposed onto the cavity flow by the blade to blade pressure field.

The  $M_{rel}$  distribution (figure 4) shows the rotor wake at  $\Theta_{rel}=0.05$  (dash-dotted line). The wake is convected into tangential direction by  $\Delta\Theta_{rel}=0.35$  from the location of the trailing edge. On the pressure side of the wake, a higher  $M_{rel}$  is detected than on the suction side. Assuming a constant relative total pressure of the rotor exit flow, this effect is induced by the static pressure field.

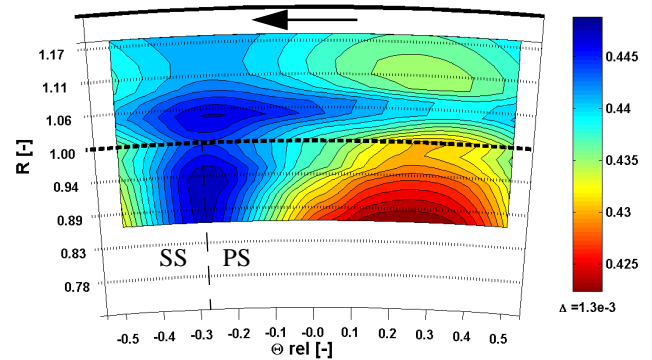


Figure 3 Non-dimensional static pressure  $C_{ps}$ , time averaged, rotor relative frame,  $Z=0.5$

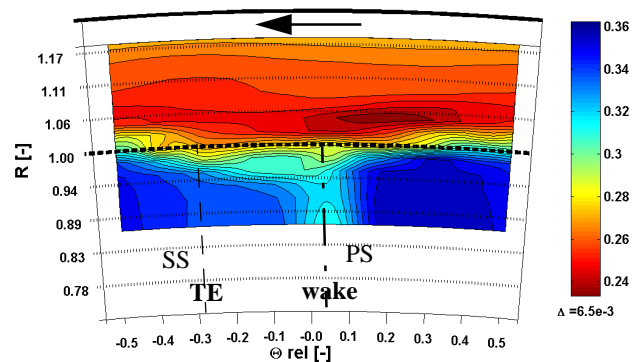


Figure 4 Relative Mach-number  $M_{rel}$ , time averaged, rotor relative frame;  $Z=0.5$

Closer to the tip radius the wake becomes wider. A band of lower  $M_{rel}$  is found between  $R=1.03$  and  $R=1.07$ , which corresponds to the leakage jet position observed in figure 2. In a region having, its centre at  $\Theta_{rel}=0.2$  and  $R=1.05$ ,  $M_{rel}$  reaches a local minimum of 0.24. The relative total pressure in the cavity is set up by the leakage jet and distributed such that the local minimum in velocity is found on the pressure side of the rotor wake. For this circumferential distribution of the leakage fluid two reasons can be named: firstly, the momentum and kinetic energy distribution of the leakage jet at the exit of the last seal and secondly, the static pressure field set up by the flow field in the main annulus including the trailing edge pressure field.

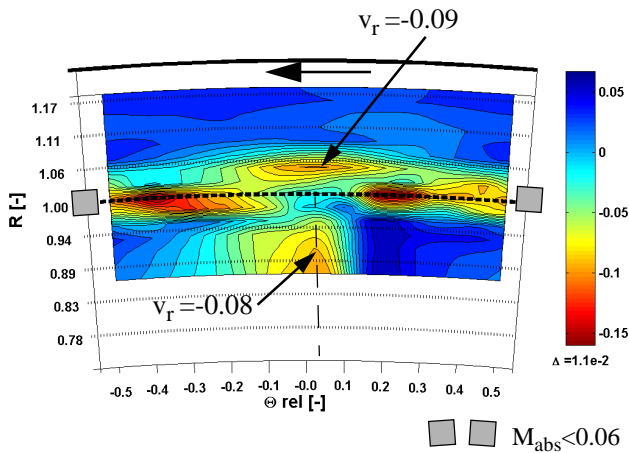


Figure 5 Non-dimensional radial velocity component, time averaged, rotor relative frame,  $Z=0.5$

Discussing the radial velocity component given in figure 5, additional details of the leakage interaction are found. The rotor wake is indicated with the dashed line. The regions of large negative radial velocities  $v_r = -0.15$  (red) are not considered for discussion. The reason for this is the fact that the error in the results for the virtual four sensor probe rapidly rises for absolute Mach-numbers higher than 0.06. The grey shaded symbols at  $R=1$  indicate a band of radial positions where the absolute Mach-number falls from 0.1 to below 0.06. This deficit of absolute velocity corresponds to the wake of the shroud. The radial velocity is negative within the region of the leakage jet ( $R=1.06$ ) having a minimum radial velocity of  $v_r = -0.09$  at the circumferential position of the wake. This value is of the same order of magnitude as the radial velocity within the wake itself ( $v_r = -0.08$ ). The leakage fluid moves out of the cavity mainly below the wake position, filling up the area of lower relative kinetic energy of the wake

### Leakage to main flow interaction

The basic components of the leakage jet to main flow interaction found in the 1% gap case in cavity 2 comprise of three points:

1) Leakage fluid migrates into the rotor wake causing the leakage streamlines to contract into the wake area. The radial migration of the leakage fluid leads to a broadening of the wake in the vicinity of the blade tip. The wake seems to attract low kinetic energy fluid.

2) The potential field of the rotor trailing edge divides the leakage sheet into distinct jets. figure 6a shows the time averaged relative velocity triangles within the relative frame of reference for the first rotor exit flow field (cavity 2). It represents the velocity vectors found with two cuts in figure 4, one at  $R=0.91$  and the other at  $R=1.06$ . The upper vectors represent the leakage jet ( $R=1.06$ ) and the lower one the main flow at  $R=0.91$ . Note, that the base of the velocity vector is representing the location of the circumferential coordinate. The arrow represents 100% of the shroud rim speed. The circles point out the base of velocity vectors, which are facing the trailing edge position of the rotor  $\Theta_{rel} = -0.25$ . The leakage mass flow is redistributed from a homogenous distribution within the last gap. A maximum of leakage mass flow is found in the mid position between the trailing edges where it forms a distinct jet (see dotted ellipse). The main flow is much less

affected by the trailing edge pressure field than the leakage jet. The main flow vectors reveal the wake of the rotor blade.

3) The potential field of the stator leading edge three-dimensionally redistributes the flow field in the absolute frame of reference. This effect is visualized in figure 6b, which presents the circumferential distribution of the absolute velocity triangles in the stator frame of reference for the 1% gap case. The diagram depicts the velocity vectors of the leakage fluid in the upper part and the velocity vectors of the main flow at  $R=0.9$  in the lower part. The velocity arrow represents 20% of the shroud rotational speed. The leading edge position of the stator is obvious in the downstream flow field of the first rotor (cavity 2), where it causes a deviation of streamlines. The circles point out the base of velocity vectors, which are facing the leading edge position of the stator at  $\Theta_{rel} = -0.22$ . Downstream of the second rotor (cavity 2') this effect is not present and the velocity vectors of the leakage jet are constant around the circumference (not shown in a diagram).

These observations are brought together in a descriptive flow model given in figure 7a. The arrows indicate the rotor passage vortex, the radial migration within the wake and the tangential redistribution of the leakage mass flow (red) due to the rotor trailing edge pressure field. The grey shaded area corresponds to the higher leakage mass flow and the blue ellipse marks the area of the radial movement of the leakage fluid out of the cavity into the wake.

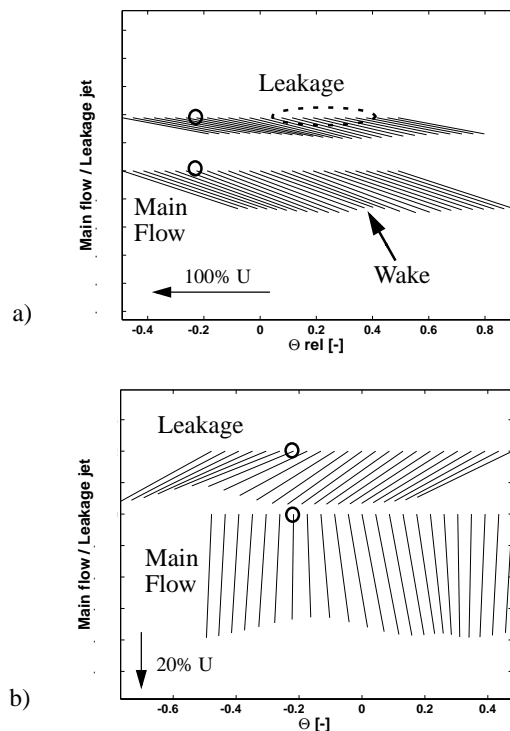


Figure 6 Time averaged velocity triangles, cavity 2: a) relative frame, b) absolute frame

### Mixing calculation

At this stage of investigation it is of interest to know the losses generated by the leakage jet mixing with the main flow. Since the

mixing is a three-dimensional process, the authors propose a 2-step mixing approach in order to capture pitch-periodic effects. From the experimental results, it is known that the radial movement of the leakage fluid (figure 5) out of the cavity occurs prior to the full mixing of the two streams. In this radial movement different flow qualities do interfere due to the fact that the flow is non-axisymmetric (wake, leakage mass distribution). Therefore, the mixing process is modelled in two steps as it is indicated in figure 7 b) through d):

1) The idealized flow field shown in figure 7b) is describing the situation depicted in figure 7a). Two areas represent the leakage and main flow each having its proper tangential variation in velocity triangles. The first mixing step is performed under constant area for each of the 20 circumferential sections of the blade pitch (figure 7b, 7c).

2) The second step is performed mixing all 20 stripes to the final mixed out situation (figure 7c, 7d).

The boundary conditions for this mixing calculation are given in table 3. The inner radius of the mixing domain  $R_i$  was set to 0.72 such, that the loss core of the stator is covered. This implies, that the mixing of the leakage jet with the main flow will be restricted to the end wall region rather than mixing with fluid at the hub. The outer radius  $R_o$  was adjusted to the leakage to main mass flow ratio. From the measurement with FRAP probes one also gains the time averaged total temperature of main and cavity flow. The leakage jet was found to have a 1.4°C higher relative total temperature than the main flow.

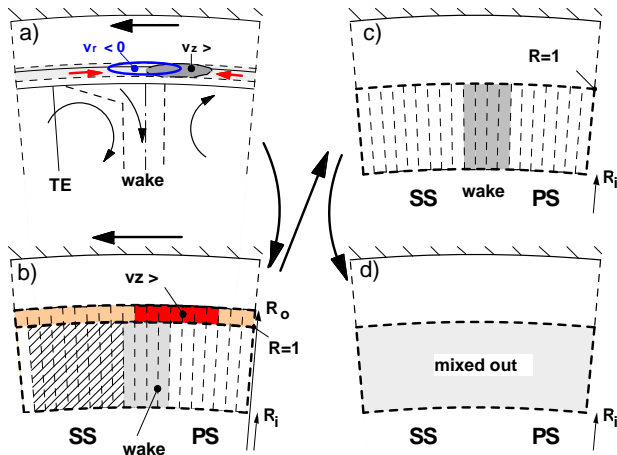


Figure 7 a) Rotor relative descriptive flow model, b) to d) 2-step mixing calculation of leakage and main flow

| $R_o - R$ [-] | $T_{rel}^o$ [°C]        | $p$ [kPa] | $\dot{m}_L/\dot{m}$ [%] |
|---------------|-------------------------|-----------|-------------------------|
| 0.028         | jet: 34.7<br>main: 33.3 | 11.0      | 1.39                    |

Table 3 Boundary conditions for mixing calculation

The mixing losses are expressed in terms of entropy rise as calculated with the entropy equation

$$\Delta s = c_p \ln \frac{\overline{T}_0}{\overline{T}_2} - R \ln \frac{\overline{p}_0}{\overline{p}_2}. \quad (1)$$

The indices refer to the stagnation values of temperature and pressure at the inlet and exit of the stage. The values of entropy are non-dimensionalized using the stage losses as derived from the performance measurements (see table 4). The mixing of the leakage jet downstream of the first stage generated 6.7% of the stage losses, where in average 22% of the loss are contributed by the mixing of different total temperature streams.

The level of mixing given in table 4 seems to be relatively high. In order to set the mixing losses found with the model in relation to a similar test case in literature, Chaluvadi et al. [12] was chosen. The test case of this publication is a single stage shrouded turbine with a seal gap clearance of around 0.7% blade height. The authors discuss the loss distribution of the stage found with experimentally based, steady CFD. They divided the flow path in loss regions, (named upstream, hub, suction side, core, pressure side, casing, downstream) and assigned percentages of blade losses to them. From this a percentage of downstream losses to stage losses can be given: Downstream of their rotor, this evaluation gives around 17% of stage losses, which includes the wake mixing as well as the vortex mixing. The maximum mixing loss resulting from the model is around 10% of stage loss including the wake and the leakage mixing. From this rough comparison it can be concluded, that the mixing model is giving reasonable results on the absolute level. Therefore, differences due to changed boundary conditions of the 2-step mixing model can be treated as a tendency and a quantification of the potential improvements.

|        | $P_{mix}$ [% stage loss] | $\Delta s_T/\Delta s$ [%] |
|--------|--------------------------|---------------------------|
| 1% gap | 6.7                      | 22                        |

Table 4 Mixing losses of cavity 2, contribution of temperature term to entropy generation

### Cavity 3 (outlet, hub)

In figure 8 the pitch-wise mass averaged results are presented and a comparison of the 0.3% and 1% gap case is given. The velocity components are made non-dimensional with the rotor hub speed. The total pressure of the cavity flow depends strongly on the gap width. A larger gap decreases the total pressure which is in conjunction with a lower tangential velocity component. A reason for this could be that the higher leakage mass flow in the 1% gap case has not fully adjusted to the circumferential speed of the rotor hub cavities. In the 0.3% gap case the tangential velocity in the cavity is much closer to the hub velocity. The axial velocity component (figure 8b) shows a mass deficit around  $R=0.05$  in the 1% gap case and a higher axial velocity at  $R=-0.08$ . The first is caused by the higher mass flow being sucked into the inlet cavity, the latter is due to the stronger leakage mass flow. The point of zero through flow  $v_z=0$  is located at  $R=-0.12$ .

Surprisingly, the radial velocity components (figure 8d) show mostly negative values. The radial migration of flow under the radial static pressure gradient is one explanation for the main flow region. However, the leakage mass flow was expected to show in average positive radial velocity components since the leakage mass flow has to leave the cavity

at some point. In the circumferential mass averaged diagram this seems to happen further downstream, e.g. at  $Z=0.8$ . A stronger outflow between  $Z=0.8$  and 1 would also explain the difference in radial velocity component at  $R=0.05$  between the two gap cases. The main flow streamlines at this point ( $Z=0.5$ ,  $R=0.05$ ) would see a greater blockage at the rotor hub, causing the streamlines to bend into the main flow again ( $\Delta v_r > 0$ )

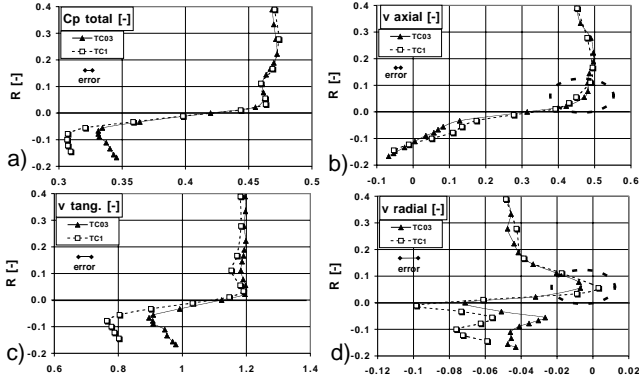


Figure 8 Pitch-wise mass-averaged,  $Z=0.5$ : a) total pressure b) axial, c) tangential, d) radial velocity components

The velocity triangles of the leakage ( $R=-0.08$ ) and the main flow ( $R=0.2$ ) for both gaps are compared in figure 9. From this, the rotor hub region can expect a negative incidence around  $\Delta\beta=-70^\circ$ . This large value might decrease, if the leakage flow passes the exit corner of the cavity, where the fluid is accelerated and deviated into streamwise direction.

Figure 10 presents the total pressure and the radial velocity component distribution at  $Z=0.5$  of the 1% gap case. The thick dashed line represents the hub radius of the blades. The thin dashed lines are indicating the stator trailing edges which also go along with a high static pressure region. The full line highlights the position of the wake. The loss core is small since the incoming boundary layer is sucked away at the hub inlet cavity. The wavy flow structure between the main and the cavity flow is showing a distinct inflow jet on the pressure side of the wake similar to what was found for cavity 4 in [8]. Below the wake position ( $\Theta=0.25$ ) the radial velocity becomes positive. This is also the region where most of the leakage flow will leave the cavity further downstream.

From these observations a short descriptive flow model can be given for this cavity (figure 11). The thin lines indicate dividing stream lines. The static pressure field set up by the high swirl and the stator trailing edges is expanding into the cavity. This has two consequences:

- 1) The leakage flow is rather pushed into the cavity rolling up into a toroidal vortex, than moving out of the cavity immediately at  $Z=0.1$ . The out flow happens further downstream around  $Z=0.9$ .
- 2) The three dimensional pressure field redistributes the leakage mass flow such, that most of it will leave the cavity at a certain circumferential position relative to the stator leading edge. Due to the convection of the wake into tangential direction both locations (wake and out flow) might coincide (e.g. at  $\Theta=0$ ).

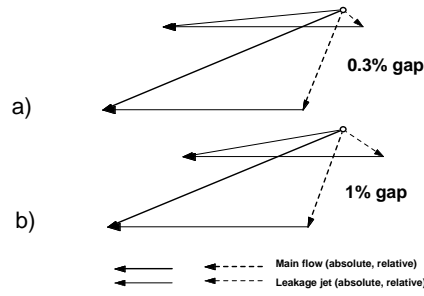


Figure 9 Pitch-wise mass-averaged velocity triangles,  $Z=0.5$ : a) 0.3% gap, b) 1% gap

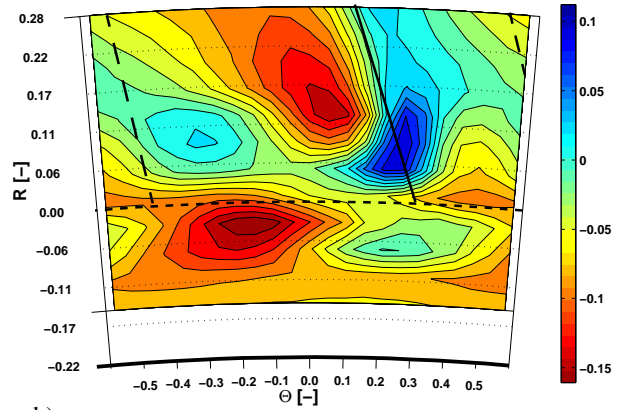
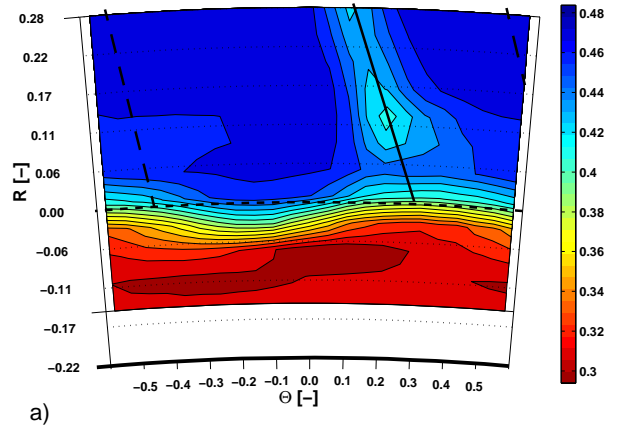


Figure 10 Downstream stator 2, 1% gap case,  $Z=0.5$ : a) total pressure, b) radial velocity component

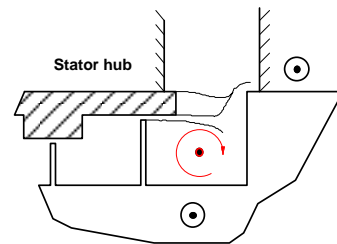


Figure 11 Flow model for cavity 3

## Cavity 4 (inlet, tip)

In an earlier publication, Pfau et al. [8] described the vortical flow structure in the inlet cavity (cavity 4) as in and out flows set up by the stator flow field. A toroidal vortex was observed moving at high tangential velocity (83% of rotor speed). This toroidal vortex was discovered to be subject to unsteady vortex stretching. In this publication further details and quantification of the flow are presented.

### Pitch-wise mass averaged results

First a short comparison of the two gap cases is given in figure 12. The diagrams show the pitch-wise mass averaged velocity profiles for the axial, radial and tangential direction.

The axial velocity component, made non-dimensional with the blade tip speed, is given in figure 12a. The over and under turning effect of the flow due to the stator passage vortex are seen in the velocity profile. The local maximum at  $R=0.8$  is caused by under turning. The over turning leads to a kink in the axial velocity profile at  $R=0.93$ . Zero through flow is found around  $R=1.06$ . The back flow component within the cavity reaches values up to 10% of the blade tip speed. Comparing this region of back flow, a significant difference between the two gap cases is found. Instead of a local strong back flow at  $R=1.16$ , the axial velocity profile linearly approaches the cavity wall in the 1% gap case. This linear profile does not indicate the presence of a second toroidal vortex close to the sealing fin as the 0.3% gap velocity profile does.

The radial velocity in figure 12b is consistent with the toroidal vortex. From the comparison of the 1% and 0.3% gap case no differences in shape is found but in absolute values some variations can be reported. The 1% gap case exhibits higher positive values in a region between 90% and 106% blade height than the 0.3% gap case. This indicates an increased radial mass flow into the cavity caused by the bigger leakage mass flow. Close to the cavity wall the trend inverts: the 0.3% gap case is characterized with higher positive values than the 1% gap case. Both toroidal vortices are cut at different axial positions relative to their centre. The strong back flow of figure 12b is moving closer to the cavity wall.

In figure 12c the over and under turning behaviour results in a local maximum and minimum of tangential velocity at  $R=0.8$  and  $R=0.93$ , respectively. Comparing the 0.3% and 1% gap cases reveals small differences close to the cavity wall and stronger ones in the main flow due to the different under and over turning characteristic of both cases. Note, that the tangential velocity of the toroidal vortex fluid is not significantly altered by the gap variation.

As the experimental results show, at least two toroidal vortices are present within the inlet cavity. Both vortices swirl at a tangential velocity of 83% of the blade tip speed around the annulus. This tangential velocity is influenced little by the gap width and depends on the operation point, i.e. the swirl of the main flow. The tangential velocity of the vortex fluid expresses the momentum balance of the inlet cavity. The centre position and strength of both vortices depend on the gap width, which is schematically displayed in figure 13. The small triangles at the cavity bottom indicate the location of the high pressure region found with the wall pressure measurements. These points are interpreted as stagnation points of the in flow passing between and driving the two toroidal vortices. Streamlines, representing the circumferentially averaged flow, are introduced in both cases. If the seal gap is opened a bigger portion of fluid flow transporting positive axial momentum is sucked into the labyrinth. Consequently, less axial

momentum needs to be redirected into radial and upstream (negative) axial momentum. The second, downstream vortex gets smaller and weaker. The toroidal vortex within the interaction zone moves into the cavity and slightly downstream, since the diameter increases and the vorticity drops.

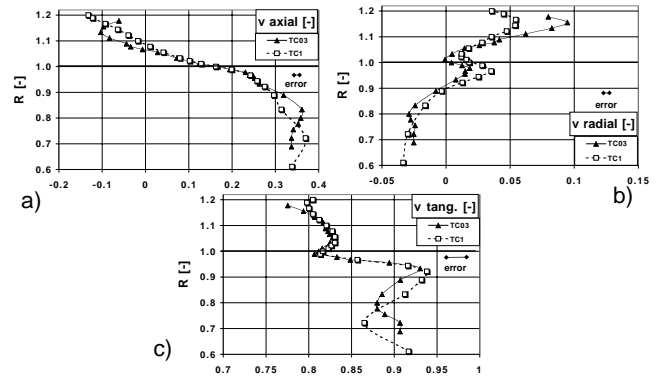


Figure 12 Pitch-wise mass averaged velocity profiles, cavity 4, 0.3% and 1% gap,  $Z=0.5$ : a) axial, b) radial, c) tangential

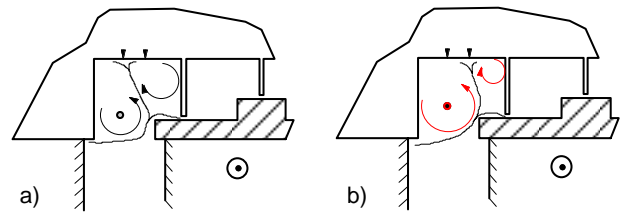


Figure 13 Vortex system, a) 0.3% gap, b) 1% gap

### Results on the interface surface

The interface surface between the cavity and the main flow is defined as a cylindrical surface with  $R=1$ . In the absolute frame of reference the radial velocity distribution shows the location of in and out flows set up by the stator flow field as presented in figure 14a. At the axial position  $Z=0.5$  a comparison between the two gap cases is given in figure 14b. The shape of the circumferential distribution of the radial velocity component is the same, but the level is shifted according to the bigger leakage mass flow being sucked into the cavity for the 1% gap case. The in flow region with positive radial velocity component is obvious. The corresponding fluid stems from the pressure side corner of the stator passage, as described in [8].

Within the relative frame the radial velocity distribution given in figure 15a shows the upstream effect of the rotor passage. The isoline of zero radial velocity is indicated with a dashed line. On the pressure side of the rotor passage fluid is pushed into the cavity, while it is sucked out on the suction side. This interaction process is an additional contributor to the torque balance of the cavity, which will be discussed in the following section. Furthermore, it alters the inflow condition to the rotor end wall region considerably. For the discussion of this effect figure 15b shows the relative stream wise vorticity distribution time averaged in the rotor relative frame of reference. The dashed line indicates the zero radial velocity isoline. The arrows indicate, that negative stream wise vorticity is sucked in to the rotor passage on

suction side. This fluid has the same rotational direction as the rotor passage vortex which develops further downstream in the passage

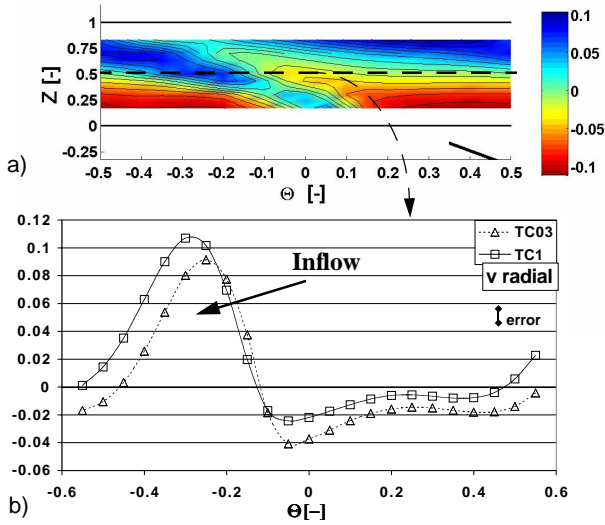


Figure 14 Radial velocity component, absolute frame: a) interface surface, R=1, 0.3% gap, b) Z=0.5, 0.3% and 1% gap

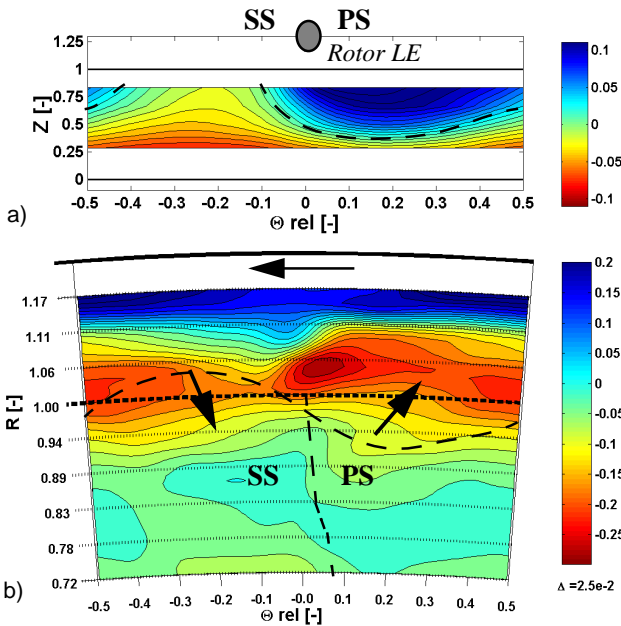


Figure 15 Relative frame: a) Radial velocity component, 0.3% gap, R=1 b) Relative stream-wise vorticity, Z=0.83

## Mass and Momentum Exchange

### Time averaged (absolute frame)

The mass and momentum exchange due to the interaction of the main flow with the open inlet cavity is investigated using the control volume as shown in figure 16a and an integration tool. The integration tool uses linear interpolation within the measurement grid. Each time

step is evaluated in a quasi-steady way. Non-slip conditions at the stationary and rotating walls are applied. The region between the nearest measurement point to the point on the wall is linearly interpolated. The integration can be performed on surfaces of constant radii, constant axial or circumferential position. In circumferential direction, pitch-periodic conditions are assumed. The boundary conditions on the inlet and exit axial plane Z=0 and Z=1 are set to the measurement values of the closest measurement plane.

The outer surface at R=1 represents the interface between main and cavity flow. The inner surface was chosen to R=0.91. At this radial location the area integration of constant radius delivers a net radial mass flow of approximately 0. For R>0.91 this integration becomes positive, for R<0.91 negative. Therefore, R=0.91 is interpreted as a dividing stream surface: Below R=0.91, the negative radial migration of the main flow dominates, above R=0.91 the flow field is affected by sucking mass into the cavity.

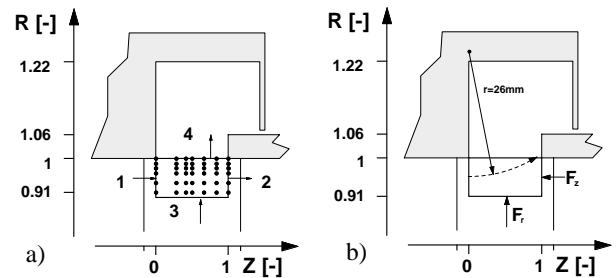


Figure 16 Control volume for mass and momentum integration: a) measurement grid, b) External forces on control volume  $F_r$ ,  $F_z$ ; radius of average streamline curvature

The results of the integration are given in table 5 representing the full annulus. Fluxes out of the control volume are counted positive and external forces on the control volume are calculated. In tangential direction the momentum flux is expressed as torque.

Considering first the sum of mass flows and fluxes in the last row of table 5, continuity is preserved within 11g/s which is 0.1% of the main mass flow. The sum of the momentum fluxes is positive in radial and negative in axial direction. Sucking mass flow into the cavity reduces the axial momentum in the end wall region, since some of the incoming axial momentum is transformed into radial momentum. In tangential direction, the sum is close to 0, since no external forces act in this direction. The components of the external force acting on the control volume are depicted in figure 16b.

| Surface i | $\dot{m}_i$ [g/s] | $F_{ir}$ [N] | $T_i$ [Nm] | $F_{iz}$ [N] |
|-----------|-------------------|--------------|------------|--------------|
| 1 (in)    | 606               | 0.5          | -24.2      | -17.1        |
| 2 (out)   | -562              | 1.8          | 22.3       | 14.2         |
| 3 (in)    | 2                 | 0.4          | -0.2       | -0.2         |
| 4 (out)   | -35               | 0.4          | 1.8        | 0.6          |
| sum       | 11                | 3.1          | -0.3       | -2.4         |

Table 5 Control volume integration according to figure 16a: mass flow and momentum fluxes on the full annulus

The mass flow passing through the control volume amounts to 6% of the main mass flow. The assumption  $\dot{m}_3 = 0$  is met to within 0.02% of the main mass flow. The net mass flow at surface 4 compares well to the leakage mass flow, which was evaluated to 37g/s. Associated to the inflow into the cavity at surface 4 is the transport of a torque of 1.8Nm.

The local radial pressure gradient across this control volume is not sufficient to keep the flow on a constant radius. Streamlines from the stator pressure side corner enter the cavity. This effect arises from the presence of a sudden area increase due to the cavity and from the sucking of the leakage mass flow. The radial equilibrium of forces acting on a circular motion is given by

$$v_z \frac{\partial v_z}{\partial z} \sin \gamma + \frac{v_z^2}{r_z} \cos \gamma - \frac{v_\Theta^2}{r} = -\frac{1}{\rho} \frac{\partial p}{\partial r} + \frac{F_r}{\rho V}, \quad (2)$$

where  $r_z$  denotes the radius of the streamline in the meridian plane. The first term describes the radial acceleration along the streamline. The second term is the radial component of the centripetal acceleration due to the meridian curvature. The third term on the left hand side represents the centripetal acceleration directed radially inward due to the main swirling flow. These three terms are balanced by the radial pressure gradient and the radial external force. In this case, eq. (2) can be simplified with the help of the experimentally based assumption that the pitch angle of the initial streamlines in surface 1 of figure 16a is approximately zero which leads to

$$\frac{v_z^2}{r_z} - \frac{v_\Theta^2}{r} = -\frac{1}{\rho} \frac{\partial p}{\partial r} + \frac{F_r}{\rho V_{CV}}. \quad (3)$$

The unknown in this equation is  $r_z$ . All other terms can be derived out of the measurement volume. The second term on the left hand side is evaluated in taking the arithmetic average of all values within the control volume according to

$$\frac{v_\Theta^2}{r} = \frac{v_{\Theta ij k}^2}{r_{ijk}}. \quad (4)$$

A representative radial pressure gradient is found in taking the pressure difference of each opposing pair of grid points, which lay on the surfaces 3 and 4. These local pressure differences are arithmetically averaged. The external radial force is taken from table 5. An average  $v_z$  on the surface 1 can be given to 19% of shroud rim speed. From this approach a representative streamline with an average meridian radius of  $r_z=26\text{mm}$  is calculated. The streamline is included in figure 16b as dotted circular arc starting at mid radial height of surface 1 with an assumed pitch angle  $\gamma=0$ . The inflow of surface 1 connects well to the area around  $Z=0.8$  of surface 4, where most of the inflow to the cavity happens (see also figure 14a).

The axial component of the external force  $F_z$  (table 5) is the result of a static pressure increase across the cavity. To verify this assumption a pressure force integration was performed taking the measured static pressure at surfaces 1 and 2. The force calculated with the pressure difference becomes -2.6N, which compares well to the control volume integration. Across the cavity opening a positive axial pressure gradient is observed. The same procedure applied to the main flow region ( $R<0.91$ ) results in a negative axial pressure gradient as expected.

Additional insight could be gained by observing the quantities associated to the in- and out-flows across surface 4, which are summarized in table 6. As much as four times of the leakage mass flow enters the cavity and convects up to 5Nm of torque, 0.9N of radial momentum flux and 1.5N of axial momentum flux. The out flow of roughly three times the leakage mass flow conveys less momentum in all three components. However, the major contribution to the radial and axial momentum balance of the control volume are found in the surfaces 1 and 2.

| Surface i         | $\dot{m}_i$ [g/s] | $F_{ir}$ [N] | $T_i$ [Nm] | $F_{iz}$ [N] |
|-------------------|-------------------|--------------|------------|--------------|
| 4 (in, $v_r>0$ )  | 127               | 0.9          | 5.1        | 1.5          |
| 4 (out, $v_r<0$ ) | -92               | -0.5         | -3.3       | -0.9         |
| sum               | 35                | 0.4          | 1.8        | 0.6          |

Table 6 Mass and momentum fluxes across surface 4, absolute frame

#### Time averaged (rotor relative frame)

The associated fluxes to the in and out flow generated by the rotor pressure field are discussed in this section. To do so, the surface integration of surface 4 in figure 16 was performed in the relative frame of reference. The radial velocity distribution of this surface is presented in figure 15a. In comparison to figure 14a, the results are restricted to five axial positions, which reduces the area covered by experimental results. The integration results are shown in table 7. The mass flow integration compares well to the results in table 6, because the time averaged radial velocity components were adjusted to the five hole probe results as found in figure 12b. The radial component of momentum fluxes is larger than in the stator relative flow field. The axial component of the momentum fluxes compares well to the results in the absolute frame of reference. The important result here is that the rotor in time average extracts torque from the cavity, since the sum of in- and out-flows is negative.

| Surface i         | $\dot{m}_i$ [g/s] | $F_{ir}$ [N] | $T_i$ [Nm] | $F_{iz}$ [N] |
|-------------------|-------------------|--------------|------------|--------------|
| 4 (in, $v_r>0$ )  | 148               | 1.6          | 1.1        | 1.4          |
| 4 (out, $v_r<0$ ) | -110              | -0.6         | -1.3       | -0.9         |
| sum               | 38                | 1.0          | -0.2       | 0.5          |

Table 7 Mass and momentum fluxes across surface 4, rotor relative

#### Unsteady fluxes

The same surface integration procedure as described in the previous sections is applied to the unsteady data set of surface 4. The integration is performed at each time step. The rotor blade passage is resolved with 106 samples. The results for radial mass flow, forces and torque are presented in figure 17. It is convenient for the discussion of the results to have the relative position of rotor and stator in mind. Therefore, two relative positions are depicted in the right part of figure 17, representing the positions of maximum ( $t/T=0.05$ ) and minimum ( $t/T=0.55$ ) mass flow into the cavity.

The lines of torque and mass flow lie on top of each other within the chosen thickness of lines (figure 17a). As torque and mass flow are coupled, both reach the minimum ( $t/T=0.55$ ) and maximum ( $t/T=0.05$ ) at the same instant of time. At the minimum net inflow, the amount of in and out fluxes ( $v_r > 0$ ,  $v_r < 0$ ) are at a minimum, too. The maximum net inflow goes along with the maximum amounts of involved fluxes. The amplitudes of the fluctuations around the time averaged values (table 6) are given in table 8.

| Surface 4 | $\dot{m}_i$ [g/s] | $F_{ir}$ [N] | $T_i$ [Nm] | $F_{iz}$ [N] |
|-----------|-------------------|--------------|------------|--------------|
| in        | $\pm 25$          | $\pm 0.45$   | $\pm 0.98$ | $\pm 0.2$    |
| out       | $\pm 15$          | $\pm 0.13$   | $\pm 0.62$ | $\pm 0.2$    |
| sum       | $\pm 16$          | $\pm 0.33$   | $\pm 0.63$ | $\pm 0.1$    |

Table 8 Mass and momentum fluxes: Amplitudes

The radial component of the momentum flux (figure 17b) reaches its minimum 15% of the blade period earlier than the mass flow and the torque. As can be derived from equation (3) the meridian curvature of the streamlines is inversely proportional to the radial external force acting on a control volume. Thus, a minimum in radial external force results in a larger radius of curvature. This in turn indicates that less streamlines are bent into the cavity. The time shift  $t/T=15\%$  could be explained with inertia effects of the streamlines to change their curvature. The net axial component of the external force acting on this surface is constant in time, since the negative and positive parts fluctuate symmetrically.

The fluctuations in mass flow, torque and momentum fluxes stem from the interaction of the stator flow field and the rotor upstream effects. At  $t/T=0.05$  the mass and torque transport is at a maximum, since the inflow area of surface 4 on the pressure side of the stator wake coincides with the upstream effect of the passage pressure side. The upstream sucking effect on the suction side of the rotor passage enhances the out flow of the cavity. Vice versa the upstream effect of the rotor passage diminishes the stator triggered in and out flows at  $t/T=0.55$ .

## SYSTEMATIC CLASSIFICATION OF OPEN CAVITIES

### Characteristics of open cavities

There are three characteristics in which the open cavities differ (see also table 9):

**D) The strength of the radial pressure gradient at the interface surface due to the swirling main flow:** Downstream of the stator the swirl angle is constantly high inducing a much stronger radial pressure gradient ( $dC_{p_s}/dR=0.02$ ) than downstream of the rotor ( $dC_{p_s}/dR=0.004$ ). The exit flow of the rotor depends on the power extraction in which the stage is working. In the case of medium loaded stages the exit swirl of the rotor is small.

**II) The location at hub or tip:** Radial pressure gradients are pointing either out of the cavity as it is the case at the tip or pointing into the cavity as at the hub. Low kinetic energy fluid migrates on lower radii according to the pressure gradient than fluid of higher kinetic energy. Therefore, the leakage fluid in cavity 3 under the influence of the radial pressure gradient set up in the main flow region, moves closer to the

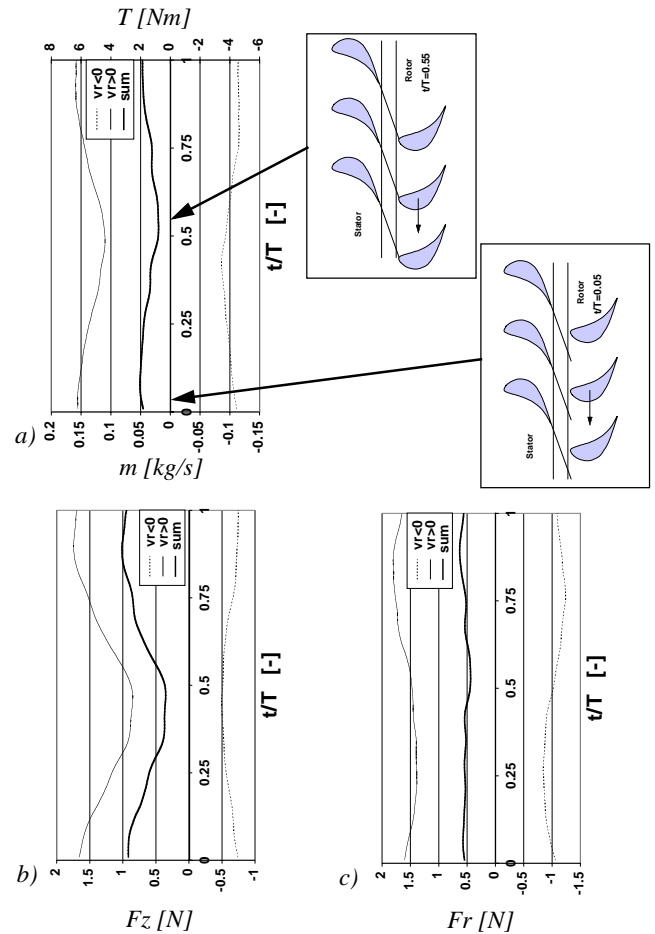


Figure 17 Unsteady fluxes, surface 4: a) mass flow, torque b) radial momentum flux, c) axial momentum flux

hub with negative radial velocity, thus forming the toroidal vortex there. The centre of the vortex is found at  $R=-0.12$ . At the tip, the low kinetic energy fluid within the cavity is sucked out of the cavity, such that the centre of the toroidal vortex in cavity 4 moves toward lower radii ( $R=1.06$ ) and the vortical flow is observed at the interface surface ( $R=1$ ).

**III) The leakage jet:** The leakage jet in the exit cavities add fluxes of axial and tangential momentum to the cavity flow. In addition, the mixing of the jet is a loss production mechanism. The leakage mass flow does no work to the rotor. This causes a higher total temperature of the leakage flow than the main flow downstream of the rotor. Downstream of the stator the total temperature of both fluxes is the same. Within the inlet cavities no jet is present, but end wall fluid is sucked into the labyrinth seal. Thus, the inlet cavity acts as a sink of axial and tangential momentum.

### Influence on main flow and performance

Each of the open cavities differ in their influence on the main flow and the performance of the machine. The effects discussed here are the change of incidence and the loss production mechanisms induced by the corresponding cavity (table 9).

**a) Incidence angle to the end wall regions of downstream blade rows:**

The leakage jet in cavity 2 and 3 causes a negative incidence due to the miss match of the velocity triangles. At the inlet to the downstream blade row the incidence angles at the end wall regions are of the order of  $-30^\circ$  and  $-70^\circ$ . Cavity 4 induces negative incidence via sucking of circumferential momentum. Evaluating the flow with the help of a control volume analysis and further modelling the flow predicts an incidence angle of  $-7^\circ$  for the 1% gap case. Cavity 1 is estimated to induce no incidence since the exit flow of the rotor, which is sucked into the hub labyrinth, has no circumferential momentum.

| No. | swirl I | Position II | Jet III         | Incidence a)                      | Loss production b)   |
|-----|---------|-------------|-----------------|-----------------------------------|--|
| 1   | -       | hub         | -               | $\Delta\alpha=0^\circ$<br>sucking | sucking of BL at hub, smaller hub loss core and secondary flows in rotor passage           |
| 2   | -       | tip         | $T_j^o > T_m^o$ | $\Delta\alpha=-30^\circ$          | Mixing of the jet with cavity and main flow<br>Jet increases. BL-thickness                 |
| 3   | ++      | hub         | $T_j^o = T_m^o$ | $\Delta\beta=-70^\circ$           | Mixing of the jet with cavity and main flow<br>Secondary flow development in rotor passage |
| 4   | ++      | tip         | -               | $\Delta\beta=-7^\circ$<br>sucking | Vortex stretching, wall friction in cavity<br>Secondary flow development in rotor          |

Table 9 Characteristics of open cavities in turbines

**b) Loss production mechanisms:** Sucking of boundary layer fluid at cavity 1 can be beneficial, since a thinner boundary layer enters the stator hub and thus less secondary flow is generated. In cavity 4 the effect of sucking may be less beneficial since the cavity is pressure loaded and interaction mass flows of up to four times the leakage mass flow do leave the cavity again. These interaction out flows then enter into the rotor tip region enhancing the secondary flow development with a sheet of positive stream-wise vorticity at the suction side of the rotor passage (see figure 15b). In addition cavity 4 contributes to the loss production via vortex stretching and enhanced wall friction due to the toroidal vortex system. In cavity 2 and 3 the leakage jet mixes with the cavity and main flow in addition of generating strong negative incidences to the downstream blade rows.

**DESIGN PROPOSALS**

In this section the gained flow understanding is used to propose design changes and to quantify a beneficial effect if possible.

**Cavity 2**

The approach for cavity 2 is to optimize the leakage mixing process. As reported in the previous section, 6.7% of the stage losses are attributable to the mixing. In a further step of investigation the mixing calculation model was used to investigate three cases of leakage mass distribution. The cases are visualized in figure 18. The upper distribution of velocity vectors belongs to the experimentally found

situation.

Case 1: Homogenous distribution of velocity vectors.

Case 2: Mirrored at  $\Theta_{rel}=0$ .

Case 3: Most of the leakage mass flow into the rotor wake.

By varying the leakage vector distribution the leakage mass flow as well as the momentum fluxes were kept constant. From this approach, an improvement of 0.1% in efficiency is predicted for the case 1 and 3 in comparison to the experiment. Case 2 does not show improvements. In case 1, downstream blade rows receive a more homogenous inflow, which is in accordance to Dawes comment about design goals in end wall regions [13]. Case 3 seems to be beneficial, since feeding the leakage flow into the wake reduces non-uniformity in the main flow and therefore reduces the mixing contribution in step 2 of the mixing model. Despite the rough assumptions applied to the mixing model, the results do indicate possible improvements.

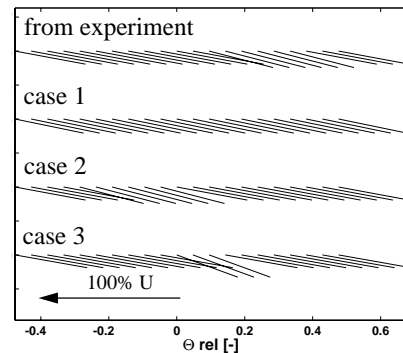


Figure 18 Rotor relative descriptive flow model and 2-step mixing calculation of leakage and main flow

In order to achieve a leakage jet distribution similar to case 3, a design modification for a non-axisymmetric shroud contour is proposed, as shown in figure 19. The gap variation around the circumference varies between completely closed at mid pitch and open at the rotor trailing edge position. The gap area is kept the same as in the 1% gap case. The leakage mass flow passing through the seal gap below the trailing edge will end up mixing with the rotor wake, when the leakage fluid leaves the cavity. Thus the leakage flow is used to reduce non-uniformities in the end wall region of the turbine.

The design of the non-axisymmetric gap depends on the re-entry behaviour of the leakage flow. A simple model is proposed to describe the circumferential position of the maximum gap relative to the rotor trailing edge ( $\Delta\Theta_{rel(G)}$ ) as depicted in figure 20. The model uses three parameters:

- 1) The characteristic length scale of the problem is the axial gap width of the exit cavity  $z_{cav}$ .
- 2) The average relative flow angle of the leakage flow from last seal gap to the re-entry into main flow  $\beta_L$ .
- 3) The relative flow angle of the main flow at the rotor tip  $\beta_T$ .

In addition, the designer has to define the location along the convective path of the wake, where it is desirable to let the leakage flow interact with the wake (wake window). These parameters combine to the non-dimensional circumferential position of the maximum gap of

$$\Theta_{relG} = \frac{z_{cav}}{p} (\tan \beta_T - 1.3 \tan \beta_L). \quad (5)$$

The local blade pitch is denoted with  $p$ . The factor 1.3 describes the geometric fact of this configuration, that the leakage jet starts at a more upstream axial position than the wake (seal gap position versus trailing edge position). For this test case and cavity the position for the maximum gap results in  $\Theta_{relG} = 0.05$ , which is very close to the trailing edge position.

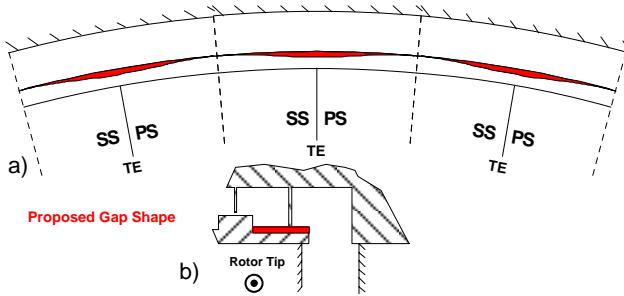


Figure 19 Non-axisymmetric shroud design in cavity 2: a) Upstream view of the last sealing gap, b) side view

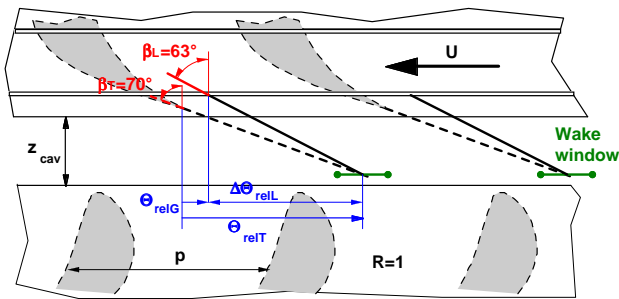


Figure 20 Simple model for shroud design

### Cavity 3

In cavity 3, the same principal as described above for cavity 2 can be applied. Thus a more uniform flow distribution would be generated at the inlet to the rotor hub and the leakage mixing losses would be reduced. As reported in [6], inserts into the exit cavities were investigated preventing the toroidal vortex to develop and guiding the leakage flow back into the main flow. The upstream effect of the rotor passage onto the leakage flow and distribution on the incoming vorticity field has been shown in the experimental results for cavity 4. In order to control the mixing and the re-entry of the leakage flow at the hub the authors propose to extend the idea of non-axisymmetric end wall contouring as described e.g. in [14] or in [15] into the exit cavity and combine it with the non-axisymmetric design of the shroud trailing edge and last seal gap. The resulting design is depicted in figure 21. The gap shape is highlighted in green. The maximum gap is shifted to the suction side of the stator passage. Thus the leakage flow can be expected to reenter into the main duct at the circumferential position of the stator wake.

Using the approach presented for cavity 2, an equation for the hub exit cavity can be given:

$$\Theta_G = \frac{z_{cav}}{p} (1.3 \tan \alpha_L - \tan \alpha_H). \quad (6)$$

Taking an average flow angle of the leakage fluid of  $\alpha_L = 75^\circ$  and the swirl angle at the hub  $\alpha_H = 67.5^\circ$ , this results in a circumferential position of the maximum gap of  $\Theta_G = 0.8$ , relative to the stator trailing edge position. The underlying assumption is, that the average flow angle of the leakage  $\alpha_L$  remains the same with the inserts. The beneficial effect will be of the same order as in cavity 2, i.e. around 0.1% absolute turbine efficiency.

The non-axisymmetric insert is designed such, that the leakage flow is guided into the rotor passage in a favorable way. The design shifts the incoming leakage fluid onto the suction side of the rotor passage. This aims at two effects:

1) The leakage fluid is found on the suction side, thus the secondary flow development in the passage due to the movement of the low kinetic energy fluid in the cross passage pressure gradient is reduced. Wall shear stresses at the end wall due to the development of a new boundary layer could be reduced.

2) The distribution of the leakage fluid to the suction side reduces the likelihood of a separation bubble at the pressure side of the rotor leading edge due to the strong negative incidence of the leakage flow. Instead of leakage fluid, a thin boundary layer of main flow fluid is hitting the rotor leading edge at the correct angle of attack.

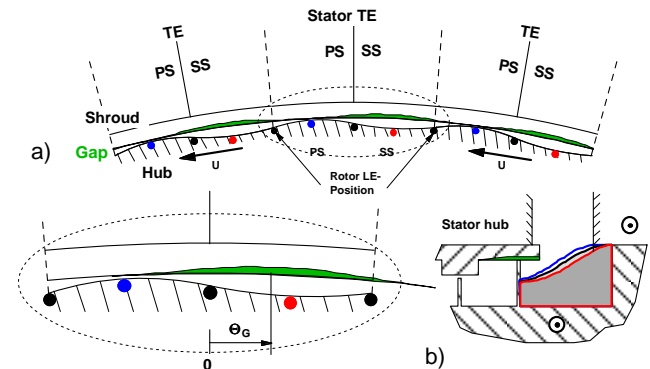


Figure 21 Non-axisymmetric shroud and cavity design, cavity 3: a) Upstream view,  $Z=0.5$ , b) side view with non-axisymmetric insert

### Cavity 4

The inlet cavity to the rotor tip labyrinth seal is subject to large in and out flows as described in detail in this publication and in [8]. Three approaches will be discussed, which are considered to be favorable in terms of loss production and reduction of unsteady interaction and secondary flows.

1) Non-axisymmetric end wall contouring in the stator passage is a promising tool to reduce secondary losses as reported in [16]. This approach has the potential to reduce the inflow and out flow due to the end wall curvature. Applied to the inlet cavity this would mean, that the end wall on the pressure side would have to be convex. The induced

static pressure drop would provide the fluid in the pressure side corner with additional kinetic energy. Thus the fluid particles tend to penetrate less into the cavity. The same target can be followed with introducing a local lean to the stator trailing edge, which would cause a local load increase. The pressure side corner fluid then would experience an additional radial force due to the imposed local static pressure gradient. A larger radius of streamline curvature is resulting from this and less amount of fluid is penetrating into the cavity.

2) The lip on the stator side of the cavity, as depicted in figure 22, is designed to reduce the circumferential wake as found in figure 12 and to turn the fluid at the edge of the toroidal vortex into axial direction. The static pressure gradients originating from the stator trailing edge and acting on the interaction zone are reduced due to the potential field decay.

3) The shroud leading edge depicted in figure 22 is designed to reduce the interaction flow across the cavity-to-main flow interface. One expected effect would be, that the radial velocity distribution as presented in figure 15a is more homogenous and the peak radial velocities are reduced. On the pressure side of the rotor passage the shroud leading edge is positioned at a higher radius than on the suction side. The effect of this is, that streamlines of a lower curvature are entering on the pressure side. Less fluid is pushed into the cavity at this point. On the suction side, the cavity fluid has to reach lower radii in order to be sucked into the rotor passage. In terms of streamline curvature, more fluid is pushed into the cavity at the suction side than on the pressure side.

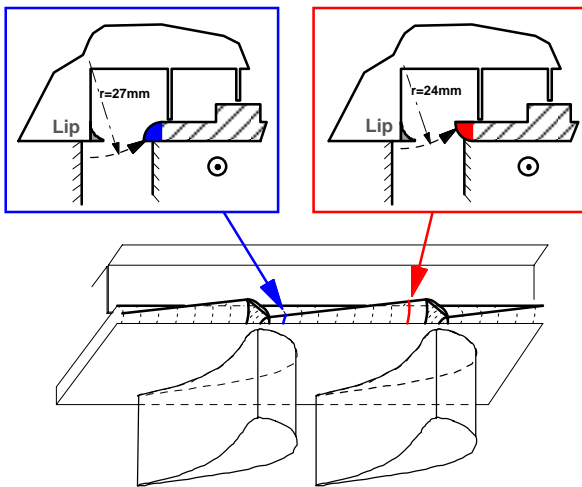


Figure 22 Shroud leading edge design for reduced rotor passage to cavity flow interaction

The design modification described above with the help of figure 22 can be inverted, i.e. it is the goal to enhance the interaction flow such, that the inlet stream wise vorticity distribution as found in figure 15b would show a higher value at the suction side to the rotor tip inlet. Consequently, the rotor passage vortex would increase its strength and change position. At first glance, this might not be a beneficial effect. But considering a designer's need to increase the rotor tip passage vortex in order to compensate incoming or downstream vorticity of the opposite sign (vortex interaction), this might be the correct approach.

## CONCLUSIONS

Detailed flow understanding is the key issue to further push the edge of the aerodynamic performance of state-of-the-art turbines. This paper presented a systematic investigation and description of the influence of large open cavities on the end wall flow region of shrouded axial turbines. This is of particular interest to low aspect ratio, high pressure stages, where secondary flows are significant. From the flow understanding design modifications have been deduced. Based on the quantitative prediction of the beneficial effect for one design modification, an optimum design suggest a potential of 0.2 to 0.5% on the overall turbine efficiency. This gain can be made through applying and optimizing all above described design modifications. The basic idea is to introduce a new degree of freedom into the shroud and cavity design: the non-axisymmetric shape. These modifications make use of the nature of the labyrinth interaction flows. Secondary flow development in downstream blade rows can be actively changed and the leakage fluid can be actively distributed. Secondary flow development within the blade rows as well as mixing losses should be optimized with the leakage flow development aiming at better turbine efficiency.

## ACKNOWLEDGMENTS

The flow measurements in the turbine were supported by the German Federal Ministry of Economy (BMWI) under file numbers 0327060D and 0327060F. The authors gratefully acknowledge AG Turbo, Alstom Power and Rolls-Royce Germany for their support and permission to publish this paper.

## REFERENCES

- [1] Denton, J.D., Johnson, C.G., 1976, "An experimental study of the tip leakage flow around shrouded turbine blades", CEBG research report CEBG-R/M/N848
- [2] Peters P., Breisig V., Giboni A., Lerner C., Pfost H., 2000, "The influence of the clearance of shrouded rotor blades on the development of the flow field and losses in the subsequent stator", 2000-GT-478, ASME Turbo Expo, May 2000, Munich
- [3] Hunter S.D., Manwaring S.R., 2000, "Endwall cavity flow effects on gaspath aerodynamics in an axial flow turbine: Part 1 - Experimental and numerical investigation, 2000-GT-651, ASME Turbo Expo, May 2000, Munich
- [4] Wallis AM, Denton JD, Demargne AAJ, 2001, "The control of shroud leakage flows to reduce aerodynamic losses in a low aspect ratio, shrouded axial flow turbine", Journal of Turbomachinery, Apr. 2001, Vol.123, pp 334-341
- [5] Anker J.E., Mayer J.F., 2002, "Simulation of the interaction of labyrinth seal leakage flow and main flow in an axial turbine", GT2002-30348, ASME Turbo Expo, June 2002, Amsterdam
- [6] Schlienger J., Pfau A., Kalfas A.I., Abhari R.S., 2003, "Effects of labyrinth seal variation on multistage axial turbine flow", GT2003-38128, ASME Turbo Expo, 16-19 June 2003, Atlanta
- [7] Pfau A., Treiber M, Sell M, Gyarmathy G, 2001, "Flow interaction from the exit cavity of an axial turbine blade row labyrinth seal", J. of Turbom., Apr. 2001, Vol.123, pp 342-352
- [8] Pfau A., Schlienger J., Rusch D., Kalfas A.I., Abhari R.S., 2003, "Unsteady Flow Interactions within the Inlet Cavity of a Turbine Rotor Tip Labyrinth Seal", GT2003-38128, ASME Turbo Expo, 16-19 June 2003, Atlanta

- [9] Sell, M., Schlienger, J., Pfau, A., Treiber, M., Abhari, R.S., 2001, "The 2-stage axial turbine test facility LISA", Proceedings of the ASME Turbo Expo, 2001-GT-492, June 4-7, New Orleans, Louisiana
- [10] Treiber, M., Kupferschmied, P., Gyarmathy, G., 1998, "Analysis of the error propagation arising from measurements with a miniature pneumatic 5-hole probe", Proc. of the 13th Symp. on measuring techniques in cascades and turbomachines, 1998, Limerick, Ireland
- [11] Pfau A., Schlienger J., Kalfas A.I., Abhari R.S., 2003, "Unsteady, 3-dimensional flow measurement using a miniature virtual 4 sensor Fast Response Aerodynamic Probe (FRAP)", GT2003-38128, ASME Turbo Expo, 16-19 June 2003, Atlanta
- [12] Chaluvadi, V.S.P., Kalfas, A.I., Baniegbal, M.R., Hodson, H.P., Denton, J.D., 2001, "Blade row interaction in a high pressure turbine", AIAA Journal of Propulsion for Power, Vol. 17, Part 4, pp. 892-901 Jul.-Aug. 2001
- [13] Dawes, W.N., VKI Lecture series (1998). "Blade row interference effects in axial turbomachinery stages: Simulation of unsteady blade row interaction with CFD: Background", February 9-12, 1998
- [14] Gregory-Smith DG, Ingram G, Jayaraman P, Harvey NW, Rose MG, 2001, "Non-axisymmetric turbine end wall profiling", Proceedings of the Institution Of Mechanical Engineers Part A, Journal of Power and Energy, Vol. 215 (A6), pp 721-734
- [15] Havakechian, S., Greim, R. (1999). "Aerodynamic design of 50 per cent reaction steam turbines", in "Development of Turbomachinery Design", edited by Denton J., IMechE, Professional Engineering Publishing Ltd., London
- [16] Harvey, N.W., Brennan, G., Newman, D.A., Rose, M.G. ( 2002). "Improving turbine efficiency using non-axisymmetric end walls: Validation in the multi-row environment and with low aspect ratio blading", GT-2002-30337, ASME Turbo Expo, June 3-6, Amsterdam, Netherlands